

Efficient ER exit and vacuole targeting of yeast Sna2p require two tyrosine-based sorting motifs

Henri-François RENARD, Didier DEMAEGD, Bérengère GUERRIAT and Pierre MORSOMME[§]

Université catholique de Louvain, Institut des Sciences de la Vie, Croix du Sud 4/15, B-1348 Louvain-la-Neuve, Belgium

[§] Corresponding author :

Tel : +32 10 47 26 23

Fax : +32 10 47 38 72

Email: pierre.morsomme@uclouvain.be

Running title : Sna2p trafficking requires two YXXØ motifs

Keywords : secretory pathway / vacuole / yeast / lipid bodies / YXXØ motif

Abbreviations : AP, adaptor proteins ; CPY, carboxypeptidase Y ; ER, endoplasmic reticulum ; LBs, lipid bodies ; PCR, polymerase chain reaction ; WT, wild type.

ABSTRACT

SNA proteins (Sensitive to Na⁺) form a membrane protein family, which, in the yeast *Saccharomyces cerevisiae*, is composed of four members, Sna1p/Pmp3p, Sna2p, Sna3p and Sna4p. In this study, we focused on the 79 residue Sna2p protein. We found that Sna2p is localized in the vacuolar membrane. Directed mutagenesis showed that two functional tyrosine motifs YXXØ are present in the C-terminal region. Each of these is involved in a different Golgi-to-vacuole targeting pathway : the tyrosine 65 motif is involved in AP-1-dependent targeting, while the tyrosine 75 motif is involved in AP-3-dependent targeting. Moreover, our data suggest that these motifs also play a crucial role in the exit of Sna2p from the ER. Directed mutagenesis of these tyrosines led to a partial redirection of Sna2p to lipid bodies, probably due to a decrease in ER exit efficiency. Sna2p is the first yeast protein in which two YXXØ motifs have been identified and both were demonstrated to be functional at two different steps of the secretory pathway, ER exit and Golgi-to-vacuole transport.

This is an Accepted Article that has been peer-reviewed and approved for publication in the *Traffic*, but has yet to undergo copy-editing and proof correction. Please cite this article as an "Accepted Article"; doi: 10.1111/j.1600-0854.2010.01070.x

INTRODUCTION

In the secretory pathway, protein export from the endoplasmic reticulum (ER) to the Golgi apparatus is mediated by the COPII complex (1,2). Exiting of membrane proteins from the ER can be facilitated by signal sequences, such as the di-acidic motifs DXD and DXE (3,4,5,6), the di-hydrophobic motifs FF, YY, LL and FY (reviewed in 7), and the tyrosine-based sorting motif YXX \emptyset (8,9,10), although there are many examples of proteins that do not possess any known export signal.

Some proteins do not exit the ER in COPII vesicles, but integrate into lipid bodies (LBs). LBs are cytosolic neutral lipid droplets (triglycerids and sterol esters) surrounded by a phospholipid monolayer (11,12). Although there are different models explaining their genesis, it is generally accepted that they bud from the ER membrane. Many monotopic membrane proteins are embedded in these LBs, and most of these are involved in lipid metabolism (13,14). LBs are not only storage sites for neutral lipid that can be used in case of energy deprivation, but also contribute to free sterol and fatty acid homeostasis in the cell, which plays a crucial role in cell structure and function : in particular, free sterols can modify membrane permeability and fluidity (15).

Once in the Golgi apparatus, proteins can be directed to different subcellular compartments, namely endosomes, vacuoles/lysosomes, plasma membrane or the extracellular medium in the case of soluble proteins. Transport between the Golgi and vacuoles/lysosomes can be mediated by different pathways with the help of adaptor protein complexes called AP complexes (16,17). In yeast, the proteins involved were first discovered by sequence homology with known AP complex proteins from other eucaryotic species (18,19,20). These heterotetrameric AP complexes are involved in cargo selection and also bind clathrin for vesicle budding.

In yeast, there are three AP complexes, AP-1, AP-2 and AP-3 (16,21). AP-1 interacts both physically and genetically with clathrin (18,20,22,23,24). This complex has been described as mediating anterograde (25,26) and/or retrograde (27) transport between the Golgi and endosomes. Because of its sequence homology with mammalian equivalents, AP-2 is thought to be involved in clathrin-dependent endocytosis from the plasma membrane to endosomes (23,24,28), although its interaction with clathrin has not yet been demonstrated. AP-3 is involved in direct transport between the Golgi and vacuoles, thus by-passing the endosomes (19,20,21,28,29). Surprisingly, this adaptor complex can act independently of clathrin (30). The AP-3-dependent pathway is also called the alkaline phosphatase pathway.

Several sorting motifs are known to interact with specific subunits of the AP complexes. These can be classified into two different groups (reviewed in 17), the "tyrosine-based" (NPXY, YXX \emptyset) and "dileucine-based" ([DE]XXXL[L]) motifs. In particular, YXX \emptyset (where \emptyset is a bulky hydrophobic residue) is able to interact with the μ subunits of AP complexes.

Sna2p is a 79 residue membrane protein from *Saccharomyces cerevisiae*. Three homologs are found in yeast, Sna1p/Pmp3p (31), Sna3p (32) and Sna4p (33). Although Pmp3p is known to play a role in maintaining the plasma membrane potential, the function of Sna2p is unknown. This protein is not essential under normal conditions. Sna2p with GFP fused to its C-terminal localizes in punctate structures (34,35). *In silico* analysis of Sna2p suggests the presence of two transmembrane domains in the N-terminal two-thirds of the molecule and a hydrophilic C-terminal cytoplasmic tail of about 25 residues.

In this study, we focused on the localization and trafficking of Sna2p. First, we showed that GFP-Sna2p is localized in the vacuolar membrane. Surprisingly, truncation of the C-terminal tail (deletion of 6, 11, 19 or 24 residues) induced a dramatic change in its localization to the plasma membrane and LBs. Directed mutagenesis showed that two functional tyrosine-based sorting motifs YXX \emptyset (\emptyset = hydrophobic residue) are present in the C-terminal tail, each involved in a different Golgi-to-vacuole targeting pathway. The tyrosine 65 motif is involved in the AP-1-dependent pathway (passing through endosomes), while the tyrosine 75 motif is involved in the AP-3-dependent pathway (direct targeting from the Golgi to vacuole, bypassing the endosomes). Moreover, our data suggest that these YXX \emptyset motifs also play a role in the exiting of Sna2p from the ER. Directed mutagenesis of the tyrosine motifs led to a partial redirection of Sna2p to LBs, probably due to a decrease in ER exit efficiency. Sna2p is the first yeast protein for which two YXX \emptyset motifs have been demonstrated to be functional : on the one hand, they are both involved at two different steps of the secretory pathway in ER exit and Golgi-to-vacuole transport and, on the other, they act in two different, but parallel, Golgi-to-vacuole targeting pathways, the AP-1- and AP-3-dependent pathways.

RESULTS

Sna2p is localized in the vacuolar membrane

Two expression systems were used, an inducible *GAL1* promoter (data not shown) or the *SNA2* endogenous promoter. Whatever the expression system used, we observed that the position of the GFP had a strong impact on Sna2p localization. When GFP was fused to the C-terminus of Sna2p (Fig. 1A, Sna2p-GFP), the protein was localized in undefined punctate structures and in the vacuolar membrane. This observation is consistent with the results in a previous report (34). However, when GFP was fused to the N-terminus of Sna2p (Fig. 1A, GFP-Sna2p), the protein was only found in the vacuolar membrane. This difference between N- and C-terminal fusions suggests the presence in the C-terminal region of important motifs for Sna2p localization. The observation that its homologs Sna3p and Sna4p have sorting motifs in the C-terminal end (32,33) suggests that this C-terminal region could also be important for Sna2p localization and, thus, that fusion of GFP to the C-terminus is not appropriate.

Sna2p contains a YXXØ motif starting at tyrosine 75

In order to identify a potential sorting motif in the Sna2p C-terminal end, we examined the localization of four truncated versions GFP-Sna2pΔ6, GFP-Sna2pΔ11, GFP-Sna2pΔ19 and GFP-Sna2pΔ24, lacking the last 6 to 24 residues. Compared to full-length Sna2p (Fig. 1A, GFP-Sna2p), the truncated forms showed a dramatic change in localization, with a strong re-localization to the plasma membrane and undefined punctate structures throughout the cytosol. Fig. 1A shows the data for GFP-Sna2pΔ6 and GFP-Sna2pΔ24, and the same behaviour was observed for the Δ11 and Δ19 forms (data not shown), whichever of the two expression systems was used.

From these results, we can conclude that a sorting motif must be present in the last six residues of Sna2p, as deletion of this region was sufficient to cause mislocalization to the plasma membrane and punctate structures. Analysis of the last six residues of Sna2p showed the presence of a potential tyrosine-based motif YXXØ, where Ø is a hydrophobic residue, which is leucine in the case of Sna2p (see Fig. 1B, YGSL sequence highlighted). Mutation of tyrosine 75 to alanine produced the same localization pattern seen with the Sna2p truncated forms (see Fig. 1A, GFP-Sna2p^{Y75A}).

These results show that Sna2p contains a functional tyrosine-based sorting motif at the level of residue 75 and that this motif is necessary for proper localization of Sna2p to the vacuolar membrane.

The absence of the Y₇₅XXØ motif redirects Sna2p to lipid bodies

When we expressed C-terminal truncated versions (GFP-Sna2pΔ6, GFP-Sna2pΔ11, GFP-Sna2pΔ19, GFP-Sna2pΔ24) or a mutated form (GFP-Sna2p^{Y75A}) of Sna2p or when we expressed Sna2p with GFP fused to its C-terminus, we observed localization in undefined punctate structures (Fig. 1A). Differential interference contrast microscopy revealed that these punctate structures always co-localized with bright dots (Fig. 1A, see white arrows), which could be lipid bodies (LBs), neutral lipid droplets (steryl esters and triacylglycerids) surrounded by a phospholipid monolayer. We examined this possibility using two different approaches.

Firstly, we performed a co-localization experiment based on fluorescence microscopy. The *sna2Δ* strain was co-transformed with two different plasmids, one carrying the *SNA2* construct fused to GFP under the control of its endogenous promoter and the other carrying *ERG6* fused to DsRed under the control of the PGK constitutive promoter (see Table II). Erg6p-DsRed is a marker of LBs used by Binns *et al.* (36). Four different *SNA2* constructs were tested in this co-localization experiment: *SNA2*-GFP, GFP-*SNA2*, GFP-*SNA2Δ6* and GFP-*SNA2*^{Y75A} (see Table II). In the case of GFP-Sna2p, no co-localization was observed with Erg6p-DsRed, as GFP-Sna2p was localized in the vacuolar membrane, while Erg6p-DsRed was found in the LBs (Fig. 2A). However, in the other cases, we observed a partial co-localization with Erg6p-DsRed (Fig. 2B, C and D, respectively), suggesting that the punctate structures are LBs. The partial co-localization was due to intracellular movement between the taking of the GFP and DsRed pictures. Fixation of the cells in 4% formaldehyde showed that co-localization of GFP-Sna2pΔ6 with Erg6p-DsRed was almost complete (Fig. 2E and F).

To confirm these results, we performed a cell fractionation experiment. As explained in the Materials and Methods, this approach led to the production of a fraction enriched in intact vacuoles and another containing purified LBs. The results of Western blot analysis of these fractions are shown in Fig. 3. Immunoblotting using anti-DsRed antibodies (Fig. 3B) showed a strong signal from LBs and a very weak signal from vacuoles. Immunoblotting using antibodies against carboxypeptidase Y (CPY), a vacuolar luminal peptidase, showed the opposite pattern (Fig. 3C). This demonstrated that the vacuoles and LBs had been separated and that mutual contamination was very low. Immunoblots using antibodies against two other membrane-specific markers, Pep12p, an endosome marker (Fig. 3D), and Bos1p, a marker of the endoplasmic reticulum (ER) (Fig. 3E), showed a slight contamination of the vacuolar fractions with other membranes and the high purity of the LB fractions. Immunoblotting using anti-GFP antibodies (Fig. 3A) showed that most of the GFP-Sna2p was found in the fraction enriched in vacuoles, whereas most of the Sna2p-GFP, GFP-Sna2pΔ6 and GFP-Sna2p^{Y75A} was found in the purified LB fraction.

In conclusion, the punctate structures observed when GFP was fused to the C-terminus of Sna2p or when the Y₇₅XXØ motif was deleted or mutated correspond to LBs.

Sna2p contains a second YXXØ motif starting at tyrosine 65

In order to explore Sna2p trafficking between the Golgi and the vacuoles in more detail, we expressed GFP-Sna2p, Sna2p-GFP, GFP-Sna2pΔ6 and GFP-Sna2p^{Y75A} in a strain deficient in LB biosynthesis. This strain (*are1Δ*, *are2Δ*, *dga1Δ*, *lro1Δ*) lacks four genes coding for enzymes involved in neutral lipid synthesis (37) and lacks LBs, but is still able to grow under normal conditions. GFP-Sna2p was still correctly addressed to the vacuolar membrane, as in the wild-type (WT) (Fig. 4A). More interestingly, the localization of Sna2p-GFP was restored to that of the WT Sna2p, i.e. localization in the vacuolar membrane (Fig. 4B). This suggests that the GFP hides a C-terminal signal involved in Sna2p ER exit efficiency (see below), but that the signal involved in Golgi-to-vacuole transport of Sna2p was less disturbed by the GFP fusion. In the case of GFP-Sna2pΔ6 (Fig. 4C) and GFP-Sna2p^{Y75A} (Fig. 4D), a part of the protein was redirected to the plasma membrane, but a signal was still present in the vacuolar membrane, showing that the Y₇₅XXØ motif alone does not explain Sna2p targeting from the Golgi to the vacuole.

These last observations suggested that another signal must be present upstream of the last 6 residues. We checked this hypothesis by expressing the truncated forms GFP-Sna2pΔ11, GFP-Sna2pΔ19 and GFP-Sna2pΔ24 in the strain

deficient in LB biosynthesis. Interestingly, none of these forms was localized to the vacuolar membrane (Fig. 4E, F and G). Together with the former results, these observations imply that a signal important for Golgi-to-vacuole transport is present between position $\Delta 11$ and $\Delta 6$ of Sna2p (residues 69 to 73). At this position in Sna2p (Fig. 1B), we find a putative phosphorylation SSSDD motif. Our experiments showed that Sna2p was phosphorylated at this level, but directed mutagenesis of this motif (triple serine mutated to triple alanine) did not influence significantly Sna2p localization (data not shown). However, upstream of SSSDD, we noted the presence of another putative YXX \emptyset motif starting at tyrosine 65 (Fig. 1B, highlighted YSHL sequence). Even though the motif is not in the last 11 residues, $\Delta 11$ truncation might affect its function because of the close proximity. In the strain deficient in LB biosynthesis, mutation of tyrosine 65 also caused mislocalization to the plasma membrane, but a signal was still present in the vacuolar membrane (Fig. 4H).

These results suggest that Sna2p contains two functional YXX \emptyset motifs. In order to verify if these motifs explained Sna2p targeting from the Golgi to the vacuole, we simultaneously mutated tyrosines 65 and 75 to alanine. In this case, all the signal was found in the plasma membrane and Sna2p Golgi-to-vacuole transport was completely abolished (Fig. 4I). We confirmed the role of the Y₆₅XX \emptyset and Y₇₅XX \emptyset motifs using a biochemical approach. The same co-fractionation experiment as that shown in Fig. 3 was used for strains expressing GFP-Sna2p, GFP-Sna2p^{Y65A}, GFP-Sna2p^{Y75A} or GFP-Sna2p^{Y65/75A} and fractions enriched in vacuoles or in LBs were analyzed by SDS-PAGE and anti-GFP Western blots. Fig. 5A again shows that the Erg6p-DsRed was concentrated in the LB fraction and the CPY signal in the vacuolar fraction, with very low mutual contamination. GFP-Sna2p signal was higher in the vacuolar fraction than in the LB fraction. However, this situation was reversed when one of the tyrosines was mutated, as the signal in the LB fraction increased, while that in the vacuolar fraction decreased, and became almost zero when both tyrosines were mutated. These results were consistent with the previous microscopic observations (Fig. 4D, H and I).

Immunodetection using antibodies raised against the 25 last residues of Sna2p showed that wild-type Sna2p was essentially localized in the vacuolar membrane (Fig. 5B) as GFP-Sna2p. This observation confirms that the fusion of GFP to the N-terminus of Sna2p has no influence on its localization. Moreover, those results show that the localization of Sna2p in normal conditions is in the vacuolar membrane and not in the LBs.

To conclude, Sna2p contains two YXX \emptyset motifs (tyrosines 65 and 75), both of which are involved in the Golgi-to-vacuole transport of Sna2p. Their simultaneous mutation completely blocks Sna2p Golgi-to-vacuole transport and Sna2p is routed to the plasma membrane.

Further characterization of YXX \emptyset motifs

In order to further characterize the YXX \emptyset motifs, we performed a systematic mutation of each residue to alanine (Fig. 6). The systematic mutagenesis on Y₆₅SHL motif showed that leucine 68 is as important as tyrosine 65 for Sna2p targeting (Fig. 6A). However, the mutation of its XX residues (serine 66 and histidine 67) had no effect on the protein localization (Fig. 6A). Therefore Y₆₅SHL fits to the canonical definition of YXX \emptyset motif. On the other side, the systematic mutagenesis performed on Y₇₅GSL motif also showed the importance of leucine 78 (Fig. 6B). However, in contrast to Y₆₅SHL motif, the mutation of XX residues of Y₇₅GSL motif had an effect on Sna2p localization. While the mutation of serine 77 showed a wild-type phenotype, the mutation of glycine 76 affected strongly the localization of Sna2p (Fig. 6B). This unexpected observation indicates an important role for glycine 76 in the motif.

Sna2p is targeted to the vacuolar membrane via AP-1- and AP-3-dependent pathways

The YXX \emptyset motif is known to interact with the protein transport machinery (17). More precisely, it can bind to the μ subunits of the heterotetrameric AP complexes involved in cargo selection and formation of transport vesicles (coat). In the yeast genome, there are four genes coding for μ subunits, namely *APM1* (AP-1 complex), *APM4* (AP-2 complex), *APM3* (AP-3 complex) and *APM2* (unknown).

In order to determine which AP complex is responsible for Sna2p targeting to the vacuolar membrane, we examined the localization of GFP-Sna2p (Fig. 7A), GFP-Sna2p^{Y65A} (Fig. 7B) and GFP-Sna2p^{Y75A} (Fig. 7C) in BY4742 strains in which each *APM* gene was deleted and, using image analysis software, quantified the plasma membrane/vacuolar membrane signal in order to have statistical data.

In the case of GFP-Sna2p, deletion of *APM2* or *APM4* had no effect on localization (data not shown), while *APM1* deletion caused a slight mislocalization to the plasma membrane (Fig. 7A, *apm1 Δ*). However, a striking effect was seen with the *APM3* deletion, which resulted in strong mislocalization to the plasma membrane (Fig. 7A, *apm3 Δ*). These results suggest that the AP-1-dependent pathway, and, more importantly, the AP-3-dependent pathway are involved in Golgi-to-vacuole targeting of Sna2p. Similar results were obtained when expression was controlled using the inducible *GAL1* promoter (data not shown). Quantification of the results confirmed these observations (Fig. 7F).

In the case of GFP-Sna2p^{Y65A} (Fig. 7B), mislocalization to the plasma membrane was observed in all strains, but was much stronger in the *apm3 Δ* strain, in which no vacuolar membrane signal was seen. Quantification of the results confirmed these observations (Fig. 7F). Moreover, the plasma membrane/vacuolar membrane signal ratio for GFP-Sna2p^{Y65A} in the WT and *apm1 Δ* strains was of the same order of magnitude as that for GFP-Sna2p in the *apm1 Δ* strain. This suggests that Y₆₅XX \emptyset is involved in Sna2p Golgi-to-vacuole targeting via the AP-1-dependent pathway.

In the case of GFP-Sna2p^{Y75A} (Fig. 7C), an even stronger mislocalization to the plasma membrane was observed in all cases, but the effect was much greater in the *apm1 Δ* strain, in which no signal was seen in the vacuolar membrane. Quantification of the results confirmed these observations (Fig. 7F). Moreover, the plasma membrane/vacuolar

membrane signal ratio for GFP-Sna2p^{Y75A} in the WT and *apm3Δ* strains was of the same order of magnitude as that for GFP-Sna2p in the *apm3Δ* strain. This result suggests that Y₇₅XXØ is involved in Sna2p Golgi-to-vacuole targeting via the AP-3-dependent pathway.

We also examined the localization of the double mutant GFP-Sna2p^{Y65/75A} in a WT strain (Fig. 7D) and that of GFP-Sna2p in a *apm1Δapm3Δ* strain (Fig. 7E). In both cases, targeting of Sna2p to the vacuolar membrane was abolished. Quantification shows that the plasma membrane/vacuolar membrane signal ratio was in the same range as that for the expression of GFP-Sna2p^{Y65A} in the *apm3Δ* strain and of GFP-Sna2p^{Y75A} in the *apm1Δ* strain (Fig. 7F).

Together, these observations suggest that the AP-1- and AP-3-dependent pathways are necessary and sufficient for Sna2p Golgi-to-vacuole transport. They also suggest that the two YXXØ motifs play different roles in Golgi-to-vacuole transport, with Y₆₅XXØ being involved in Sna2p transport via the AP-1-dependent pathway and Y₇₅XXØ in Sna2p transport via the AP-3-dependent pathway.

In complementary experiments, XX residues of both motifs were mutated. Epifluorescence microscopy pictures were taken (data not shown) and quantification was carried out (Fig. 7F). Firstly, serine and histidine residues from the Y₆₅SHL motif were respectively mutated in glycine and serine as in the Y₇₅GSL motif (S66G/H67S mutations). Secondly, glycine and serine residues from the Y₇₅GSL were respectively mutated in serine and histidine as in the Y₆₅SHL motif (G76S/S77H mutations). Those two mutated forms of Sna2p were expressed in the WT strain (data not shown), and in the *apm1Δ* and the *apm3Δ* strains (Fig. 7F). The aim of this experiment was to test if one of the two YXXØ motifs could be converted in and replace the other. Quantification shows that the plasma membrane/vacuolar membrane signal ratio of GFP-Sna2p^{S66G/H67S} in the *apm1Δ* strain was in the same range as that for the expression of GFP-Sna2p in the *apm1Δ* strain. The ratio of GFP-Sna2p^{G76S/S77H} in the *apm3Δ* strain was in the same range as that for the expression of GFP-Sna2p in the *apm3Δ* strain. Those results show again that the Y₆₅SHL motif is AP-1 specific, while the Y₇₅GSL is AP-3 specific.

In the case of GFP-Sna2p^{S66G/H67S} in the *apm3Δ* strain, the value of the ratio was between those of GFP-Sna2p in the *apm3Δ* and the *apm1Δapm3Δ* strains. This intermediate phenotype indicates that the mutations S66G and H67S do not abolish completely the function of tyrosine 65 motif, and that the AP-1 complex is still able to interact partially with this motif. In contrary, the mutations G76S and S77H abolish completely the function of tyrosine 75 motif. This result is consistent with the observation that glycine 76 is important for the function of this motif (Fig. 6B). Combined mutations of the XX residues of one motif and the tyrosine of the other (GFP-Sna2p^{S66G/H67S/Y75A} and GFP-Sna2p^{Y65A/G76S/S77H}) almost completely abolished targeting of Sna2p to the vacuolar membrane.

The Y₆₅XXØ and Y₇₅XXØ motifs play a role in Sna2p ER exit efficiency

We had shown that mutation of the YXXØ motifs was sufficient to partially redirect Sna2p to LBs. Moreover, LBs are formed at the level of the ER membrane. These facts suggested the hypothesis that the YXXØ motifs are involved in Sna2p ER exit efficiency : when they are mutated or deleted, Sna2p ER export may be slower, and, rather than staying in the ER, it is loaded into nascent LBs, probably because of its hydrophobic properties. YXXØ motif involvement in ER exit has been reported for Emp46p in yeast (9) and VSV-G in mammalian cells (8,38).

In order to check this hypothesis, we used a double strategy. On the one hand, we blocked the ER exit of GFP-Sna2p, which is localized in the vacuolar membrane under normal conditions, and, on the other, we tried to force ER exit of Sna2p forms known to re-localize into LBs (Sna2p-GFP, Sna2p^{Y65A}-GFP, Sna2p^{Y75A}-GFP and Sna2p^{Y65/75A}-GFP) by addition of a DXE export motif.

For the first strategy, we blocked ER exit using a *sec18^{ts}* strain. At the permissive temperature (25°C), the strain behaves normally, but switching to the restrictive temperature (37°C) activates the *sec18* mutation and blocks ER exit. In the WT strain, GFP-Sna2p was mainly localized in the vacuolar membrane at both 25°C and 37°C (Fig. 8A). However, in the *sec18^{ts}* strain, it was found in the vacuolar membrane at 25°C, but was strongly re-routed to LBs when the cells were incubated for 30 minutes at 37°C (Fig. 8B). Moreover, when this strain was returned to 25°C for 2 h, GFP-Sna2p was again able to exit the ER and the LB signal was progressively lost (Fig. 8B). These results strongly suggest that Sna2p re-localization to LBs is the consequence of a decrease in ER exit efficiency.

In the second strategy, we forced ER exit by addition of a DXE motif by fusing the last nine amino acids of Sys1p protein, containing a functional DXE motif (4), to the C-terminus of Sna2p-GFP and Sna2p-GFP with mutated tyrosines. In contrast to Sna2p-GFP, which showed strong re-localization to LBs, Sna2p-GFP-DXE was found in the vacuolar membrane (Fig. 9A). This demonstrates that re-localization to LBs is abolished when ER exiting is forced and the DXE motif is able to make up for the dysfunction of the YXXØ motifs hidden by the addition of GFP. When the DXE motif was fused to Sna2p^{Y65A}-GFP, Sna2p^{Y75A}-GFP or Sna2p^{Y65/75A}-GFP, no signal was observed in LBs (Fig. 9B, C and D : + DXE) in contrast to the non-DXE controls (Fig. 9B, C and D : - DXE). This shows the importance of the YXXØ motifs for efficient Sna2p ER exit. Moreover, these constructions can be used to analyze the role of the YXXØ motifs in Golgi exit. In the case of Sna2p^{Y65A}-GFP-DXE and Sna2p^{Y75A}-GFP-DXE, a signal was observed in the plasma membrane and vacuolar membrane. However, when both motifs were mutated (Sna2p^{Y65/75A}-GFP-DXE), all the protein re-localized to the plasma membrane. These results confirmed the importance of the Y₆₅XXØ and Y₇₅XXØ motifs for Sna2p Golgi-to-vacuole transport and were consistent with our previous observations (Fig. 4D, H and I).

We cannot exclude the possibility that the mutations or the truncations in the C-terminal extension of Sna2p could affect its folding. This misfolding could consequently slower the exit of Sna2p from the ER and increase its degradation rate.

However, we observed that the degradation rate of GFP-Sna2p is not significantly affected by Y65/75A mutations when protein synthesis is blocked with cycloheximide (Fig. 10). The same observation was made in the strain H1246 lacking lipid bodies biosynthesis (data not shown). This strengthens the hypothesis that YXXØ motifs are important for Sna2p ER exit.

Taken together, these results suggest that the Y₆₅XXØ and Y₇₅XXØ motifs allow efficient Sna2p ER exit. Their mutation or deletion triggers a partial re-localization of Sna2p to LBs. This is probably due to a decrease in Sna2p ER exit efficiency causing the protein to be blocked in the ER, where it might be inserted into nascent LBs due to its hydrophobic properties.

DISCUSSION

In this study, we found that Sna2p was localized in the vacuolar membrane and that two functional tyrosine-based sorting motifs YXXØ were necessary for its proper localization. Hiding these motifs by fusing GFP to the C-terminus, truncation of the C-terminal end or mutation of the tyrosine residues caused re-localization into LBs. Our data suggest that the two YXXØ motifs are important for efficient Sna2p ER exit. The localization in LBs is probably a consequence of inefficient ER exit when one or both YXXØ motifs are mutated. Moreover, localization analysis in strains in which different *APM* genes were deleted revealed that Sna2p reached the vacuolar membrane by two parallel AP-pathways, the AP-1- and AP-3-dependent pathways. Our data showed that the Y₆₅XXØ motif was responsible for AP-1-dependent targeting of Sna2p to the vacuolar membrane, while Y₇₅XXØ was involved in Sna2p AP-3-dependent targeting. Besides Y₆₅ and Y₇₅, we demonstrated that Ø residues (L₆₈ and L₇₈) are also crucial for Sna2p targeting. In general, XX residues are less important than tyrosine and Ø residues for the function of those motifs. However, while Y₆₅SHL corresponds exactly to the canonical definition of YXXØ motif, we observed that glycine 76 of Y₇₅GSL motif is important for Sna2p targeting. Moreover, we showed that the XX mutations – that convert one motif in the other (S66G/H67S or G76S/S77H) – do not change the specificity of each tyrosine for AP-1 or AP-3 pathways. Other features are probably important for the AP-specificity of a tyrosine motif as its distance from the membrane domain or the nature of flanking residues.

Re-localization to LBs is linked to some features of the putative transmembrane domain

The re-localization of Sna2p to LBs was quite puzzling, as recognition of the YXXØ motif takes place at the trans-Golgi level (17), whereas LB budding occurs earlier in the secretory pathway at the level of the ER membrane (11,12). We could possibly hypothesize that this localization occurs "by default". When both YXXØ motifs are mutated, Sna2p would no longer bind to AP complexes at the level of the trans-Golgi and this would result in its accumulation in the secretory pathway as far back as the ER membrane. At this level, as it is a hydrophobic protein, we could imagine that it would be loaded by default into nascent LBs. However, we think that accumulation along the secretory pathway is not the real cause of this re-localization. Our results showed that both YXXØ motifs played a role in ER exit (Fig. 9), as reported for Emp46p in yeast (9) or VSV-G in mammalian cells (8,38). The absence of these motifs could decrease the ER exit efficiency of Sna2p, favouring its redirection into LBs.

This tendency to re-localize to LBs is not unique to Sna2p, but is a property of the whole family. When we performed co-localization experiments using Pmp3p-GFP and Erg6p-DsRed, we noted that some of the Pmp3p was also localized in LBs (unpublished data). Furthermore, we observed that Sna3p-GFP and Sna4p-GFP were able to re-localize to LBs when ER exit was blocked using a *sec18^{fs}* strain (unpublished data). This localization feature seems to be linked to the predicted N-terminal transmembrane domain of these proteins, where they show a high similarity. The localization of Sna2p is thus the result of a competition between the properties of the C-terminal region YXXØ motifs, which are important for ER exit and vacuolar localization, and those of the putative transmembrane domain, thought to play a role in LB localization.

All SNA proteins contain conserved prolines in their putative transmembrane domain, a feature that is relatively common, as about 25 % of transmembrane helices contain prolines (39). Prolines could introduce kinks in hydrophobic helices and provide SNAs with the required topology to direct them to LBs.

Several proteins contain a proline knot, which is important for their targeting to LBs. This has been reported in the plant protein oleosin (40,41), the core proteins of hepatitis C virus and GB virus-B in mammalian cells (42) and caveolin-1 (44). In all these cases, the proline knot probably influences the packing of hydrophobic helices by introducing helical kinks that break their linearity. The topology models suggested by the above authors (40,41,43,44) present these proteins as monotopic, the hydrophobic helices being embedded in only one leaflet of the phospholipid bilayer due to the kink. This topology is ideal for localization into LBs.

Even though SNA proteins do not show sequence similarity with oleosins or caveolins, they do share two features, i.e. the presence of prolines in the hydrophobic domain and their ability to reach LBs. The presence of prolines in the putative transmembrane domain of SNA proteins might give them a specific topology that could favour their localization to LBs (see Sna2p topology model, Fig. 11). However, we cannot exclude that both membrane-spanning and non-spanning conformations are functional. The exact mechanism and physiological meaning of re-localization to LBs remain to be investigated.

Both YXXØ motifs of Sna2p play a role in ER exit efficiency and in Golgi-to-vacuole transport

GFP-Sna2p was localized in the vacuolar membrane, but re-localization into the plasma membrane and LBs was observed when at least one of the two YXXØ motifs was deleted or mutated, confirming their importance for proper localization of Sna2p. When both motifs were mutated, all of the protein that reached the trans-Golgi network was targeted to the plasma membrane: the plasma membrane is a common “by default” localization for membrane proteins that possess no specific targeting motif.

The YXXØ motif has already been reported in many proteins from a wide range of eukaryotic organisms, such as human, rat, *Drosophila* and protozoa (17). It was first discovered in the early nineties as a signal for the rapid degradation (endocytosis) of a bovine plasma membrane receptor (45,46). Now, it is also known to mediate the targeting of certain proteins from the Golgi to vacuoles/lysosomes (17) and also ER exit, as mentioned above. In yeast, very few proteins have been shown to possess a functional YXXØ sorting motif. Only three have been reported in the literature : Yck3p, a vacuolar membrane-bound casein kinase (47), Nyv1p, a v-snare component of the vacuolar SNARE complex involved in vesicle fusion (48) and Emp46p (9), a Golgi protein involved in glycoprotein secretion. The YXXØ motifs of Yck3p and Nyv1p are involved in their direct targeting from the Golgi apparatus to the vacuolar membrane through the AP-3-dependent pathway, thus bypassing the endosomes. In contrast, the YXXØ motif of Emp46p is involved in ER exit. Sna2p is consequently the fourth member of the YXXØ motif yeast proteins. However, Sna2p has new characteristics that make it unique (Fig. 11) : 1°) it contains two, rather than one, functional YXXØ motifs and both are involved in two successive steps of the secretory pathway, ER exit and Golgi-to-vacuole transport ; 2°) each of these motifs is responsible for Sna2p Golgi-to-vacuole targeting via a different, but parallel, AP-pathway, the AP-1-dependent pathway in the case of the Y₆₅XXØ motif and the AP-3-dependent pathway in the case of the Y₇₅XXØ motif.

MATERIALS AND METHODS

Strains, plasmids, media and growth conditions

The yeast strains used are listed in Table I. The BY4741 or BY4742 background strains were from the Euroscarf systematic deletion library (kanamycin deletion cassette). The double deletant *apm1Δ apm3Δ* was obtained by crossing the single deletants BY4742 *apm1Δ* and BY4741 *apm3Δ*. The SCY62 and H1246 strains were provided by Pr Sten Stymne (37). RH448 and RH5464 were provided by Howard Riezman (University of Geneva).

The plasmids used are listed in Table II. Two different promoters were used for the expression of the *SNA2* constructs, the inducible *GAL1* promoter (p416) and the *SNA2* endogenous promoter (pRS416-*pSNA2*). The *SNA2* endogenous promoter is the 500 bp fragment located upstream of the *SNA2* open reading frame in the BY4742 genome and was amplified by the polymerase chain reaction (PCR) using specific primers. All GFP constructions were produced in two steps. Firstly, *GFP* was amplified from p416-*TPI-SNA2-GFP* by PCR with specific primers and cloned into the p416 or pRS416-*pSNA2* plasmid. Secondly, the *SNA2* fragment was amplified from the same plasmid with specific primers to produce complete or truncated versions of *SNA2* (*SNA2-ΔCt6*, *SNA2-ΔCt11*, *SNA2-ΔCt19* and *SNA2-ΔCt24*) and cloned into the GFP-carrying plasmids p416 or pRS416-*pSNA2*. *SNA2* N-terminal and C-terminal GFP fusions were produced in this way. The same method was used to produce plasmids carrying *SNA2* with the mutations as described in Table 2. The DXE motif was added using specific primers including the coding sequence for the last 9 residues of Sys1p (QLKDLESQI).

All constructs were completely sequenced. Faststart High Fidelity PCR polymerase and Phusion DNA Polymerase were purchased from Roche Applied Science and Finnzymes, respectively. PCR primers were obtained from Sigma. All restriction and modification enzymes were from New England Biolabs. The *E. coli* strain used for plasmid amplification was JM109 and was grown on standard media supplemented with 100 µg/ml of ampicillin for plasmid selection.

Non-transformed yeast cells were cultured at 28°C in YD medium (2 % glucose, 2 % yeast extract). Cells transformed with plasmids carrying constitutive promoters were grown in YNB minimal medium containing 0.7 % yeast nitrogen base (Difco) and 2 % glucose and supplemented with all amino acids except those used as selection markers for plasmid maintenance. Cells transformed with plasmids carrying the inducible *GAL1* promoter were cultured in YNB minimal medium containing 0.7 % yeast nitrogen base (Difco), 2 % D-raffinose pentahydrate (Sigma) and 0.05 % glucose, and supplemented with all amino acids except those used as selection markers. Induction of expression was triggered by addition of 2 % galactose for 2 h, then the cells were harvested by centrifugation and resuspended in pre-warmed YD medium for repression, which was continued for 2 h. The thermosensitive strain *sec18^{ts}* (RH5465) was cultured at 25°C (permissive temperature), then transferred to 37°C (restrictive temperature) for 30 min to activate the *sec18* mutation.

Transformation was performed with lithium acetate following the method of Gietz *et al.* (49).

Fluorescence microscopy, signal quantification and co-localization

Yeast cells were observed in exponential phase using a Leica DMR epifluorescence microscope with a 100x oil immersion objective. Pictures were taken with an Orca AG Hamamatsu digital CCD camera driven by Wasabi 2.0 software. Leica GFP and Texas Red filters were used, respectively, for GFP and DsRed pictures. GFP signal quantification was performed using Hokawo 2.1 software. For co-localization experiments, yeast cells co-expressing proteins fused to GFP or DsRed were harvested in exponential phase and GFP and Texas Red pictures were taken successively. When indicated, cells were fixed before observation: cultures were treated with 4% formaldehyde for 10 min, harvested, resuspended in fixation buffer (0.1 M K₂HPO₄, pH 6.5, 0.5 mM MgCl₂, 3.7% formaldehyde), incubated for

2 h at room temperature, washed three times in washing buffer (0.1 M K₂HPO₄, pH 6.5, 1.2 M sorbitol) and observed as above.

Isolation of lipid bodies

The isolation of lipid bodies was adapted from Leber *et al.* (50). Yeast cells, grown at 28°C in 500 ml of minimal medium, were harvested at OD ~ 2.5 by centrifugation at 5000xg for 5 min. The cells were washed in 100 ml of spheroplasting buffer (0.7 M sorbitol, 10 mM Tris-HCl, pH 7.4, 50 mM DTT), and centrifuged as above, then the pellets were resuspended in 2 ml of spheroplasting buffer per g of cells, and zymolyase 20T (Seikagaku Corp., Tokyo, Japan) was added (2.5 mg per g of cells) and the mixture incubated for 45 min at 30°C. All subsequent steps were at 4°C and 1 mM phenylmethylsulfonyl fluoride (PMSF) and a protease inhibitor cocktail (4 µg/ml of leupeptin, aprotinin, antipain, pepstatin and chymostatin) were added to all buffers. Spheroplasts were harvested by centrifugation at 5000xg for 5 min, washed with 15 ml of spheroplasting buffer, and centrifuged as above, then the pellets were resuspended as 0.3 g of cells per ml in breaking buffer (10 mM MES-Tris, pH 6.9, 12 % w/w Ficoll 400, 0.2 mM Na₂EDTA). The spheroplasts were homogenized using 20-30 strokes of a Dounce homogenizer and an equal volume of breaking buffer was added for dilution, then the mixture was transferred to a 38 ml Ultra-Clear™ centrifugation tube and overlaid with an equal volume of breaking buffer. The sample was then centrifuged for 60 min at 120,000xg in an SW-32 Ti swing-out rotor (Beckman) and a floating layer, mainly composed of intact vacuoles and LBs, was recovered, gently resuspended in an equal volume of breaking buffer using a Dounce homogenizer, transferred to a 38 ml Ultra-Clear™ centrifugation tube and overlaid with an equal volume of 8 % Ficoll buffer [10 mM MES-Tris, pH 6.9, 8 % w/w Ficoll 400 (Sigma), 0.2 M Na₂EDTA]. After centrifugation for 60 min at 120,000xg in an SW-32 Ti rotor (Beckman), the floating layer was again harvested and gently resuspended (Dounce homogenisation) in an equal volume of 8 % Ficoll buffer containing 0.6 M sorbitol, transferred to a 38 ml Ultra-Clear™ centrifugation tube and overlaid with an equal volume of 0.25 M sorbitol buffer (10 mM MES-Tris, pH 6.9, 0.25 M sorbitol, 0.2 mM Na₂EDTA). After a final centrifugation for 60 min at 120,000xg in an SW-32 Ti rotor (Beckman), the floating layer, enriched in highly pure LBs, was recovered, resuspended in 200 µl of 0.25 M sorbitol buffer and stored at -80°C. The pellet at the bottom of the tube, which was enriched in intact vacuoles, was washed once with 2 ml of 0.25 M sorbitol buffer and resuspended in 100 µl of sample buffer (0.32 M Tris-HCl, pH 6.8, 8 % SDS, 40 % glycerol, 0.02 % bromophenol blue). All samples resuspended in solubilization buffer were boiled for 10 min, then volumes of samples corresponding to approximately 1/8 of each recovered fraction were subjected to SDS-PAGE.

Protein degradation assay

Yeast strains (SCY62 or H1246) expressing GFP-Sna2p or GFP-Sna2p^{Y65/75A} were precultured overnight at 28°C in YD medium. The next morning, 30 ml YD cultures were inoculated at OD 0.3, and grown until OD 0.7-0.8. Cycloheximide was added to a final concentration of 100 µg/ml in culture medium. After cycloheximide addition, an equal number of cells was collected at time 0, 30, 60, 120 and 180 min. Total cell lysates were prepared as following. Harvested cells were resuspended in 500 µl of culture medium. 50 µl of 1.85 M NaOH supplemented with 2% 2-mercaptoethanol were added, mixed, and cells were incubated for 10 min on ice. Afterwards, 50 µl of 50% TCA were added, mixed, and cells were incubated for 15 min on ice. Cell lysates were then centrifuged during 5 min at 12,000xg. Supernatants were discarded, pellets were resuspended in 70 µl of a 50:50 mix of sample buffer (see above) : 1 M Tris base and boiled for 10 min. 5 µl of solubilized pellets were subjected to SDS-PAGE for further analysis via western blotting.

Western blotting

Proteins were separated by SDS-PAGE and transferred to a PVDF membrane (Millipore, Billerica, USA) using a semi-dry transfer system (Bio-Rad) in 50 mM Tris, 40 mM glycine, 1.3 mM SDS, 20 % methanol. The blots were blocked either at room temperature for at least 45 min or overnight at 4°C in blocking buffer (20 mM Tris-HCl, pH 7.6, 150 mM NaCl, 6 % w/v low fat dried milk, 0.5 % v/v Tween 80), then were incubated with primary antibody for 2 h at room temperature or overnight at 4°C in TBS-Tween (20 mM Tris-HCl, pH 7.6, 150 mM NaCl, 0.1 % v/v Tween 80) containing 0.5 % w/v low fat dried milk. After three washes with TBS-Tween, the blots were incubated for 1 h at room temperature with secondary antibody coupled to horseradish peroxidase in TBS-Tween. Bound antibodies were revealed using a BM Chemiluminescence Blotting kit (Roche Applied Science). The emitted light was captured with a KODAK 4000R Image Station, driven by KODAK Molecular Imaging Software v4.0.0, which was also used for quantification analysis.

The primary antibodies used were mouse anti-GFP (40 ng/ml, Roche Applied Science), rabbit anti-DsRed (1:1000, Clontech), rabbit anti-CPY (1:1000, H. Riezman), mouse anti-Pep12p (0.5 µg/ml, Invitrogen), rabbit anti-Bos1p (1:1000, C. Barlowe), purified rabbit anti-Sna2p (1:500), rabbit anti-Sna3p (1:200) and rabbit anti-Cdc48p (1:1000, M. Ghislain). Rabbit polyclonal anti-Sna2p and anti-Sna3p antibodies were raised respectively against the 28-C-terminal residues of Sna2p and the 66-C-terminal residues of Sna3p expressed in *E. coli* as a fusion product with the glutathione-S-transferase (pGEX, GE Healthcare Life Sciences). The secondary antibodies were anti-mouse IgG and anti-rabbit IgG antibodies (Biognost International).

Acknowledgements

We thank W. Pokrzywa for providing plasmids, S. Mussenge for technical assistance and all members of our group for support and critical reading of the manuscript. We also thank Pr S. Szymne for providing the strains lacking LB biosynthesis, Pr H. Riezman for providing the *sec18^{fs}* strain and anti-CPY antibodies, Pr M. Ghislain for providing anti-Cdc48p antibodies and Pr J.M. Goodman for providing the pRS315-PGK-ERG6-mDsRed plasmid. H.-F. Renard is a

Research Fellow at the Fonds National de la Recherche Scientifique (Belgium). This work was funded by the Interuniversity Attraction Poles Program – Belgian Science Policy, the “Communauté française de Belgique-Actions de Recherches Concertées (grant #ARC-0510-329), the FRS-FNRS and a grant (CDA) from the Human Frontier Science Program Organization.

REFERENCES

1. Bonifacino JS, Glick BS. The Mechanisms of Vesicle Budding and Fusion. *Cell* 2004;116:153-166.
2. Sato K, Nakano A. Mechanisms of COPII vesicle formation and protein sorting. *FEBS Lett* 2007;581(11):2076-2082.
3. Nishimura N, Bannykh S, Slabough S, Matteson J, Altschuler Y, Hahn K, Balch WE. A Di-acidic (DXE) Code Directs Concentration of Cargo during Export from the Endoplasmic Reticulum. *J Biol Chem* 1999;274(22):15937-15946.
4. Votsmeier C, Gallwitz D. An acidic sequence of a putative yeast Golgi membrane protein binds COPII and facilitates ER export. *EMBO J* 2001;20(23):6742-6750.
5. Epping EA, Moyer-Rowley WC. Identification of Interdependent Signals Required for Anterograde Traffic of the ATP-binding Cassette Transporter Protein Yor1p. *J Biol Chem* 2002;277(38):34860-34869.
6. Malkus P, Jiang F, Schekman R. Concentrative sorting of secretory cargo proteins into COPII-coated vesicles. *J Cell Biol* 2002;159(6):915-921.
7. Otte S, Barlowe C. The Erv41p-Erv46p complex: multiple export signals are required in trans for COPII-dependent transport from the ER. *EMBO J* 2002;21(22):6095-6104.
8. Sevier CS, Weisz OA, Davis M, Machamer CE. Efficient Export of the Vesicular Stomatitis Virus G Protein from the Endoplasmic Reticulum Requires a Signal in the Cytosolic Tail That Includes Both Tyrosine-based and Di-acidic Motifs. *Mol Biol Cell* 2000;11:13-22.
9. Sato K, Nakano A. Emp47p and Its Close Homolog Emp46p Have a Tyrosine-containing Endoplasmic Reticulum Exit Signal and Function in Glycoprotein Secretion in *Saccharomyces cerevisiae*. *Mol Biol Cell* 2002;13:2518-2532.
10. Heineman TC, Connolly P, Hall SL, Assefa D. Conserved cytoplasmic domain sequences mediate the ER export of VZV, HSV-1, and HCMV gB. *Virology* 2004;328:131-141.
11. Zweglick D, Athenstaedt K, Daum G. Intracellular lipid particles of eukaryotic cells. *Biochim Biophys Acta* 2000;1469:101-120.
12. Czabany T, Athenstaedt K, Daum G. Synthesis, storage and degradation of neutral lipids in yeast. *Biochim Biophys Acta* 2007;1771:299-309.
13. Athenstaedt K, Zweglick D, Jandrositz A, Kohlwein SD, Daum G. Identification and Characterization of Major Lipid Particle Proteins of the Yeast *Saccharomyces cerevisiae*. *J Bacteriol* 1999;181(20):6441-6448.
14. Thiele C, Spandl J. Cell biology of lipid droplets. *Curr Opin Cell Biol* 2008;20:378-385.
15. Wagner A, Grillitsch K, Leitner E, Daum G. Mobilization of steryl esters from lipid particles of the yeast *Saccharomyces cerevisiae*. *Biochim Biophys Acta* 2009;1791:118-124.
16. Robinson MS, Bonifacino JS. Adaptor-related proteins. *Curr Opin Cell Biol* 2001;13:444-453.
17. Bonifacino JS, Traub LM. Signals for Sorting of Transmembrane Proteins to Endosomes and Lysosomes. *Annu Rev Biochem* 2003;72:395-447.
18. Stepp JD, Pellicena-Palle A, Hamilton S, Kirchhausen T, Lemon SK. A Late Golgi Sorting Function for *Saccharomyces cerevisiae* Apm1p, but not for Apm2p, a Second Yeast Clathrin AP Medium Chain-Related Protein. *Mol Biol Cell* 1995;6:41-58.
19. Cowles CR, Odorizzi G, Payne GS, Emr SD. The AP-3 Adaptor Complex Is Essential for Cargo-Selective Transport to the Yeast Vacuole. *Cell* 1997;91:109-118.
20. Panek HR, Stepp JD, Engle HM, Marks KM, Tan PK, Lemmon SK, Robinson LC. Suppressors of YCK-encoded yeast casein kinase 1 deficiency define the four subunits of a novel clathrin AP-like complex. *EMBO J* 1997;16(14):4194-4204.
21. Bowers K, Stevens TH. Protein transport from the late Golgi to the vacuole in the yeast *Saccharomyces cerevisiae*. *Biochim Biophys Acta* 2005;1744:438-454.
22. Phan HL, Finlay JA, Chu DS, Tan PK, Kirchhausen T, Payne GS. The *Saccharomyces cerevisiae* APS1 gene encodes a homolog of the small subunit of the mammalian clathrin AP-1 complex: evidence for functional interaction with clathrin at the Golgi complex. *EMBO J* 1994;13(7):1706-1717.
23. Yeung BG, Phan HL, Payne GS. Adaptor Complex-independent Clathrin Function in Yeast. *Mol Biol Cell* 1999;10:3643-3659.
24. Yeung BG, Payne GS (2001) Clathrin Interactions with C-Terminal Regions of the Yeast AP-1 β and γ Subunits are Important for AP-1 Association with Clathrin Coats. *Traffic* 2: 565-576.

25. Ha SA, Torabinejad J, DeWald DB, Wenk MR, Lucast L, De Camilli P, Newitt RA, Aebersold R, Northwehr SF. The Synaptojanin-like Protein Inp53/Sjl3 Functions with Clathrin in a Yeast TGN-to-Endosome Pathway Distinct from the GGA Protein-dependent Pathway. *Mol Biol Cell* 2003;14:1319-1333.
26. Phelan JP, Millson SH, Parker PJ, Piper PW, Cooke FT. Fab1p and AP-1 are required for trafficking of endogenously ubiquitylated cargoes to the vacuole lumen in *S. cerevisiae*. *J Cell Sci* 2006;119:4225-4234.
27. Valdivia RH, Baggott D, Chuang JS, Schekman RW. The Yeast Clathrin Adaptor Protein Complex 1 Is Required for the Efficient Retention of a Subset of Late Golgi Membrane Proteins. *Dev Cell* 2002;2:283-294.
28. Odorizzi G, Cowles CR, Emr SD. The AP-3 complex: a coat of many colours. *Trends Cell Biol* 1998;8:282-288.
29. Darsow T, Burd CG, Emr SD. Acidic Di-leucine Motif Essential for AP-3-dependent Sorting and Restriction of the Functional Specificity of the Vam3p Vacuolar t-SNARE. *J Cell Biol* 1998;142(4):913-922.
30. Vowels JJ, Payne GS. A dileucine-like sorting signal directs transport into an AP-3-dependent, clathrin-independent pathway to the yeast vacuole. *EMBO J* 1998;17(9): 2482-2493.
31. Navarre C, Goffeau A. Membrane hyperpolarization and salt sensitivity induced by deletion of PMP3, a highly conserved small protein of yeast plasma membrane. *EMBO J* 2000;19(11):2515-2524.
32. Stawiecka-Mirota M, Pokrzywa W, Morvan J, Zoladek T, Haguenaer-Tsapis R, Urban-Grimal D, Morsomme P. Binding to Rsp5p targets to the endosomal pathway the yeast Sna3p, a protein ubiquitylated with Lysine-63-linked chains. *Traffic* 2007;8:1280-1296.
33. Pokrzywa W, Guerriat B, Dodzian J, Morsomme P (2009) Dual sorting of the *Saccharomyces cerevisiae* protein Sna4p. *Eukaryot Cell* 8(3): 278-286.
34. Reggiori F, Pelham HRB. Sorting of proteins into multivesicular bodies: ubiquitin-dependent and -independent targeting. *EMBO J* 2001;20(18):5176-5186.
35. Huh WH, Falvo JV, Gerke LC, Carroll AS, Howson RW, Weissman JS, O'Shea EK. Global analysis of protein localization in budding yeast. *Nature* 2003;425:686-691.
36. Binns D, Januszewski T, Chen Y, Hill J, Markin VS, Zhao Y, Gilpin C, Chapman KD, Anderson RGW, Goodman JM. An intimate collaboration between peroxisomes and LB. *J Cell Biol* 2006;173(5):719-731.
37. Sandager L, Gustavsson MH, Ståhl U, Dahlqvist A, Wiberg E, Banas A, Lenman M, Ronne H, Stymne S. Storage lipid synthesis is non-essential in yeast. *J Biol Chem* 2002;277(8):6478-6482.
38. Aridor M, Fish KN, Bannykh S, Weissman J, Roberts TH, Lippincott-Schwartz J, Balch WE. The Sar1 GTPase Coordinates Biosynthetic Cargo Selection with Endoplasmic Reticulum Export Site Assembly. *J Cell Biol* 2001;152(1):213-229.
39. Cordes FS, Bright JN, Sansom MSP. Proline-induced Distortions of Transmembrane Helices. *J Mol Biol* 2002;323:951-960.
40. Chen JCF, Tzen JTC. An in vitro System to Examine the Effective Phospholipids and Structural Domain for Protein Targeting to Seed Oil Bodies. *Plant Cell Physiol* 2001;42(11):1245-1252.
41. Abell BM, Hahn M, Holbrook LA, Moloney MM. Membrane topology and sequence requirements for oil body targeting of oleosin. *Plant J* 2004;37:461-470.
42. Hope RG, Murphy DJ, McLauchlan J. The Domains Required to Direct Core Proteins of Hepatitis C Virus and GB Virus-B to Lipid Droplets Share Common Features with Plant Oleosin Proteins. *J Biol Chem* 2002;277(6):4261-4270.
43. Ostermeyer AG, Ramcharan LT, Zeng Y, Lublin DM, Brown DA. Role of the hydrophobic domain in targeting caveolin-1 to lipid droplets. *J Cell Biol* 2004;164(1):69-78.
44. Ostermeyer AG, Paci JM, Zeng Y, Lublin DM, Munro S, Brown DA. Accumulation of Caveolin in the Endoplasmic Reticulum Redirects the Protein to Lipid Storage Droplets. *J Cell Biol* 2001;152(5):1071-1078.
45. Canfield WM, Johnson KF, Ye RD, Gregory W, Kornfeld S. Localization of the Signal for Rapid Internalization of the Bovine Cation-independent Mannose 6-Phosphate/Insulin-like Growth Factor-II Receptor to Amino Acids 24-29 of the Cytoplasmic Tail. *J Biol Chem* 1991;266(9):5682-5688.
46. Jadot M, Canfield WM, Gregory W, Kornfeld S. Characterization of the Signal for Rapid Internalization of the Bovine Cation-independent Mannose 6-Phosphate/Insulin-like Growth Factor-II Receptor. *J Biol Chem* 1992;267(5):11069-11077.
47. Sun B, Chen L, Cao W, Roth AF, Davis NG. The Yeast Casein Kinase Yck3p Is Palmitoylated, then Sorted to the Vacuolar Membrane with AP-3-dependent Recognition of a YXXΦ Adaptor Sorting Signal. *Mol Biol Cell* 2004;15:1397-1406.
48. Wen W, Chen L, Wu H, Sun X, Zhang M, Banfield DK. Identification of the Yeast R-SNARE Nyv1p as a novel Longin Domain-containing Protein. *Mol Biol Cell* 2006;17:4282-4299.
49. Gietz RD, St Jean A, Woods RA, Schiestl RH. Improved method for high efficiency transformation of intact yeast cells. *Nucleic Acids Res* 1992;20(6):1425.

- 50.** Leber R, Zinser E, Zellnig G, Paltauf F, Daum G. Characterization of Lipid Particles of the Yeast, *Saccharomyces cerevisiae*. *Yeast* 1994;10:1421-1428.
- 51.** Sikorski RS, Hieter P. A system of shuttle vectors and yeast host strains designed for efficient manipulation of DNA in *Saccharomyces cerevisiae*. *Genetics* 1989;122(1):19-27.
- 52.** Mumberg D, Müller R, Funk M. Regulatable promoters of *Saccharomyces cerevisiae*: comparison of transcriptional activity and their use for heterologous expression. *Nucleic Acids Res* 1994;22(25):5767-5768.

TABLES

Table I : Strains used in this study

Strain	Genotype	Source
BY4742	<i>Mata his3Δ1 leu2Δ0 lys2Δ0 ura3Δ0</i>	Euroscarf
BY4742 <pmp3δ< p=""></pmp3δ<>	<i>Mata his3Δ1 leu2Δ0 lys2Δ0 ura3Δ0 pmp3::KanMX4</i>	Euroscarf
BY4742 <p>sna2Δ</p>	<i>Mata his3Δ1 leu2Δ0 lys2Δ0 ura3Δ0 sna2::KanMX4</i>	Euroscarf
BY4742 <p>sna3Δ</p>	<i>Mata his3Δ1 leu2Δ0 lys2Δ0 ura3Δ0 sna3::KanMX4</i>	Euroscarf
BY4742 <p>sna4Δ</p>	<i>Mata his3Δ1 leu2Δ0 lys2Δ0 ura3Δ0 sna4::KanMX4</i>	Euroscarf
BY4742 <p>apm1Δ</p>	<i>Mata his3Δ1 leu2Δ0 lys2Δ0 ura3Δ0 apm1::KanMX4</i>	Euroscarf
BY4742 <p>apm2Δ</p>	<i>Mata his3Δ1 leu2Δ0 lys2Δ0 ura3Δ0 apm2::KanMX4</i>	Euroscarf
BY4741 <p>apm3Δ</p>	<i>Mata his3Δ1 leu2Δ0 lys2Δ0 ura3Δ0 apm3::KanMX4</i>	Euroscarf
BY4742 <p>apm4Δ</p>	<i>Mata his3Δ1 leu2Δ0 lys2Δ0 ura3Δ0 apm4::KanMX4</i>	Euroscarf
BY <i>apm1Δapm3Δ</i>	<i>Mata his3Δ1 leu2Δ0 met15Δ0 ura3Δ0 apm1::KanMX4 apm3::KanMX4</i>	This study
SCY62	<i>Mata ADE2 can1-100 his3-11,15 leu2-3,112 trp1-1 ura3-1</i>	Ref. (37)
H1246	<i>Mata ADE2 can1-100 are1Δ::HIS3 are2Δ::LEU2 dga1Δ::KanMX4 lro1Δ::TRP1 ura3-1</i>	Ref. (37)
RH448	<i>Mata his4-619 leu2 ura3 lys2 bar1-1</i>	H. Riezman
RH5465	<i>Mata sec18^{ts} leu2 trp1 ura3 bar1-1</i>	H. Riezman

Table II : Plasmids used in this study

Plasmid	Genotype	Source
pRS416	<i>CEN, URA3</i>	Ref. (51)
p416	<i>CEN, URA3, GAL1 promoter</i>	Ref. (52)
pRS416- <i>TPI-SNA2-GFP</i>	<i>CEN, URA3, TPI1 promoter, SNA2-GFP</i>	Ref. (34)
pRS315- <i>PGK-ERG6-mDsRed</i>	<i>CEN, LEU2, PGK promoter, ERG6-mDsRed</i>	Ref. (36)
p416- <i>SNA2-GFP</i>	<i>CEN, URA3, GAL1 promoter, SNA2-GFP</i>	This study
p416- <i>GFP-SNA2</i>	<i>CEN, URA3, GAL1 promoter, GFP-SNA2</i>	This study
p416- <i>GFP-SNA2Δ6</i>	<i>CEN, URA3, GAL1 promoter, GFP-SNA2-ΔCt6</i>	This study
p416- <i>GFP-SNA2Δ11</i>	<i>CEN, URA3, GAL1 promoter, GFP-SNA2-ΔCt11</i>	This study
p416- <i>GFP-SNA2Δ19</i>	<i>CEN, URA3, GAL1 promoter, GFP-SNA2-ΔCt19</i>	This study
p416- <i>GFP-SNA2Δ24</i>	<i>CEN, URA3, GAL1 promoter, GFP-SNA2-ΔCt24</i>	This study
p416- <i>GFP-SNA2^{Y75A}</i>	<i>CEN, URA3, GAL1 promoter, GFP-SNA2-Y75A</i>	This study
pRS416- <i>pSNA2-SNA2-GFP</i>	<i>CEN, URA3, SNA2 endogenous promoter, SNA2-GFP</i>	This study
pRS416- <i>pSNA2-GFP-SNA2</i>	<i>CEN, URA3, SNA2 endogenous promoter, GFP-SNA2</i>	This study
pRS416- <i>pSNA2-GFP-SNA2Δ6</i>	<i>CEN, URA3, SNA2 endogenous promoter, GFP-SNA2-ΔCt6</i>	This study
pRS416- <i>pSNA2-GFP-SNA2Δ11</i>	<i>CEN, URA3, SNA2 endogenous promoter, GFP-SNA2-ΔCt11</i>	This study
pRS416- <i>pSNA2-GFP-SNA2Δ19</i>	<i>CEN, URA3, SNA2 endogenous promoter, GFP-SNA2-ΔCt19</i>	This study
pRS416- <i>pSNA2-GFP-SNA2Δ24</i>	<i>CEN, URA3, SNA2 endogenous promoter, GFP-SNA2-ΔCt24</i>	This study
pRS416- <i>pSNA2-GFP-SNA2^{Y65A}</i>	<i>CEN, URA3, SNA2 endogenous promoter, GFP-SNA2-Y65A</i>	This study
pRS416- <i>pSNA2-GFP-SNA2^{S66A}</i>	<i>CEN, URA3, SNA2 endogenous promoter, GFP-SNA2^{S66A}</i>	This study
pRS416- <i>pSNA2-GFP-SNA2^{H67A}</i>	<i>CEN, URA3, SNA2 endogenous promoter, GFP-SNA2^{H67A}</i>	This study
pRS416- <i>pSNA2-GFP-SNA2^{L68A}</i>	<i>CEN, URA3, SNA2 endogenous promoter, GFP-SNA2^{L68A}</i>	This study
pRS416- <i>pSNA2-GFP-SNA2^{Y75A}</i>	<i>CEN, URA3, SNA2 endogenous promoter, GFP-SNA2^{Y75A}</i>	This study
pRS416- <i>pSNA2-GFP-SNA2^{G76A}</i>	<i>CEN, URA3, SNA2 endogenous promoter, GFP-SNA2^{G76A}</i>	This study
pRS416- <i>pSNA2-GFP-SNA2^{S77A}</i>	<i>CEN, URA3, SNA2 endogenous promoter, GFP-SNA2^{S77A}</i>	This study
pRS416- <i>pSNA2-GFP-SNA2^{L78A}</i>	<i>CEN, URA3, SNA2 endogenous promoter, GFP-SNA2^{L78A}</i>	This study
pRS416- <i>pSNA2-GFP-SNA2^{Y65/Y75A}</i>	<i>CEN, URA3, SNA2 endogenous promoter, GFP-SNA2^{Y65A/Y75A}</i>	This study
pRS416- <i>pSNA2-SNA2-GFP-DXE</i>	<i>CEN, URA3, SNA2 endogenous promoter, SNA2-GFP-DXE</i>	This study
pRS416- <i>pSNA2-GFP-SNA2-DXE</i>	<i>CEN, URA3, SNA2 endogenous promoter, GFP-SNA2-DXE</i>	This study
pRS416- <i>pSNA2-GFP-SNA2Δ6-DXE</i>	<i>CEN, URA3, SNA2 endogenous promoter, GFP-SNA2Δ6-DXE</i>	This study
pRS416- <i>pSNA2-GFP-SNA2^{Y75A}-DXE</i>	<i>CEN, URA3, SNA2 endogenous promoter, GFP-SNA2^{Y75A}-DXE</i>	This study
pRS416- <i>pSNA2-SNA2^{Y65A}-GFP-DXE</i>	<i>CEN, URA3, SNA2 endogenous promoter, SNA2^{Y65A}-GFP-DXE</i>	This study
pRS416- <i>pSNA2-SNA2^{Y75A}-GFP-DXE</i>	<i>CEN, URA3, SNA2 endogenous promoter, SNA2^{Y75A}-GFP-DXE</i>	This study
pRS416- <i>pSNA2-SNA2^{Y65/Y75A}-GFP-DXE</i>	<i>CEN, URA3, SNA2 endogenous promoter, SNA2^{Y65A/Y75A}-GFP-DXE</i>	This study
pRS416- <i>pSNA2-GFP-SNA2^{S66G/H67S}</i>	<i>CEN, URA3, SNA2 endogenous promoter, GFP-SNA2^{S66G/H67S}</i>	This study
pRS416- <i>pSNA2-GFP-SNA2^{G76S/S77H}</i>	<i>CEN, URA3, SNA2 endogenous promoter, GFP-SNA2^{G76S/S77H}</i>	This study
pRS416- <i>pSNA2-GFP-SNA2^{S66G/H67S/Y75A}</i>	<i>CEN, URA3, SNA2 endogenous promoter, GFP-SNA2^{S66G/H67S/Y75A}</i>	This study
pRS416- <i>pSNA2-GFP-SNA2^{Y65A/G76S/S77H}</i>	<i>CEN, URA3, SNA2 endogenous promoter, GFP-SNA2^{Y65A/G76S/S77H}</i>	This study
pRS416- <i>pSNA2-GFP-SNA2^{S69A/S70A/S71A}</i>	<i>CEN, URA3, SNA2 endogenous promoter, GFP-SNA2^{S69A/S70A/S71A}</i>	This study

LEGENDS

Figure 1. GFP-Sna2p localization in the vacuolar membrane depends on the Y₇₅XXØ motif.

A. Sna2p C-terminal truncated/mutated forms fused to GFP re-localize to punctate structures and the plasma membrane. The SCY62 strain was transformed with pRS416-*pSNA2-SNA2-GFP*, pRS416-*pSNA2-GFP-SNA2*, pRS416-*pSNA2-GFP-SNA2Δ6*, pRS416-*pSNA2-GFP-SNA2Δ24* or pRS416-*pSNA2-GFP-SNA2^{Y75A}*. The white arrows indicate that the punctate structures in the GFP pictures co-localize with the bright punctate structures in the Nomarski pictures.

B. Sequence of Sna2p. The two transmembrane domains (TM1 and TM2) predicted using TMHMM software are shown boxed. The various Sna2p C-terminal truncated forms are indicated below the sequence; these are Δ6, Δ11, Δ19 and Δ24 with the C-terminal 6, 11, 19 or 24 residues deleted, respectively. The two YXXØ motifs (Y₆₅SHL and Y₇₅GSL) are shown shaded. Scale bar indicates 2 μm.

Figure 2. The absence of the Y₇₅XXØ motif redirects Sna2p to lipid bodies. Fluorescence microscopy of the BY4742 *sna2Δ* strain co-transformed with plasmid pRS315-*PGK-ERG6-mDsRed* and (A) pRS416-*pSNA2-GFP-SNA2*, (B) pRS416-*pSNA2-SNA2-GFP*, (C) pRS416-*pSNA2-GFP-SNA2Δ6* or (D) pRS416-*pSNA2-GFP-SNA2^{Y75A}*. E and F: the same strains as in A and C fixed with 4% formaldehyde for 2 h prior to observation. Scale bar indicates 2 μm.

Figure 3. Sna2p is enriched in the lipid bodies fraction in the absence of the Y₇₅XXØ motif. Proteins from a highly pure LB fraction (LB) and a fraction enriched in vacuoles (V) prepared from BY4742 *sna2Δ* co-transformed as in Fig. 2 were separated by SDS-PAGE and transferred to a PVDF membrane for Western blot analysis. The constructs expressed are indicated above each lane. The blots were incubated with antibodies against (A) GFP, (B) DsRed, (C) CPY, (D) Pep12p or (E) Bos1p. F. SDS-PAGE : 11% gel stained with Coomassie blue used as the loading control.

Figure 4. The Y_{65A} and Y_{75A} mutations prevent Sna2p targeting to the vacuolar membrane in a *are1Δare2Δdga1Δlro1Δ* strain. The quadruple deleted strain (H1246) lacking LBs was transformed with one of the SNA2 constructs fused to GFP. The corresponding WT strain (SCY62) was also co-transformed with pRS315-*PGK-ERG6-DsRed*. A. GFP-Sna2p ; B. Sna2p-GFP ; C. GFP-Sna2pΔ6 ; D. GFP-Sna2p^{Y75A} ; E. GFP-Sna2pΔ11 ; F. GFP-Sna2pΔ19 ; G. GFP-Sna2pΔ24 ; H. GFP-Sna2p^{Y65A} ; I. GFP-Sna2p^{Y65/75A}. Scale bar indicates 2 μm.

Figure 5. Sna2p targeting to the vacuolar membrane is abolished when both the Y₆₅XXØ and Y₇₅XXØ motifs are mutated.

Proteins from highly pure LB fraction (LB) and a fraction enriched in vacuoles (V) prepared from different strains were separated by SDS-PAGE and transferred to a PVDF membrane for Western blot analysis.

A. BY4742 *sna2Δ* co-transformed as in Fig. 4A, D, H and I. The constructs expressed are indicated above each lane. The blots were incubated with antibodies against GFP, DsRed or CPY.

B. BY4742 WT transformed with pRS315-*PGK-ERG6-DsRed*. The blots were incubated with antibodies against Sna2p, DsRed or CPY.

Figure 6. Tyrosine and leucine residues of YXXØ motifs are crucial for the targeting of Sna2p to the vacuolar membrane.

The BY4742 *sna2Δ* strain was co-transformed with pRS315-*PGK-ERG6-DsRed* and pRS416-*pSNA2-GFP-SNA2* where each residue of YXXØ motifs were respectively mutated to alanine : **A.** Y₆₅SHL motif : mutations Y65A, S66A, H67A and L68A ; **B.** Y₇₅GSL motif : mutations Y75A, G76A, S77A and L78A. Scale bar indicates 2 μm.

Figure 7. Sna2p Golgi-to-vacuole transport is mediated by AP-1 and AP-3 complexes.

A-C. Expression of GFP-Sna2p, GFP-Sna2p^{Y65A} or GFP-Sna2p^{Y75A} in the WT, *apm1Δ* or *apm3Δ* strains. Scale bar indicates 2 μm.

D. Expression of GFP-Sna2p^{Y65/75A} in the WT strain.

E. Expression of GFP-Sna2p in the double deletant *apm1Δ apm3Δ* strain.

F. Quantification of GFP signals in the plasma and vacuolar membranes suggests that Y₆₅XXØ is responsible for Sna2p targeting via the AP-1-dependent pathway, while Y₇₅XXØ is responsible for Sna2p targeting via the AP-3-dependent pathway. GFP signals were quantified in the plasma and vacuolar membranes in the strains shown in A to E, and also in the *apm1Δ* and *apm3Δ* strains expressing GFP-Sna2p^{S66G/H67S} or GFP-Sna2p^{G76S/S77H}, and in the WT strain expressing the triple mutants GFP-Sna2p^{S66G/H67S/Y75A} or GFP-Sna2p^{Y65A/G76S/S77H}. The plasma membrane/vacuolar membrane ratio calculated. For each strain, 30-60 cells from two different clones were analyzed. The error bars represent the 95% confidence interval. On the histogram, ratios in zone I are not significantly different from that for GFP-Sna2p expressed in the WT strain, ratios in zone II are not significantly different from that for GFP-Sna2p expressed in the *apm1Δ* strain, ratios in zone III are not significantly different from that for GFP-Sna2p expressed in the *apm3Δ* strain and ratios in zone IV are not significantly different from that for GFP-Sna2p expressed in the *apm1Δ apm3Δ* double deleted strain.

Figure 8. Blocking of ER exit forces GFP-Sna2p to re-localize to lipid bodies.

A. GFP-Sna2p was expressed in the WT strain (RH448) and localization was observed after culture at 25°C (permissive temperature) or at 25°C, followed by 30 min at 37°C (restrictive temperature).

B. GFP-Sna2p was expressed in the *sec18^{ts}* strain (RH5465) and localization was observed after culture at 25°C or at 25°C followed by 30 min at 37°C. After incubation for 30 min at 37°C, the cells were returned to 25°C for 1 or 2 h. Scale bar indicates 2 μm.

Figure 9. Addition of a DXE ER exit motif to Sna2p-GFP compensates for the dysfunction of the YXXØ motifs.

All constructions were expressed in the BY4742 *sna2Δ* strain. The left panels show localization without DXE and the right panels those with DXE. **A.** Sna2p-GFP; **B.** Sna2p^{Y65A}-GFP; **C.** Sna2p^{Y75A}-GFP and **D.** Sna2p^{Y65/75A}-GFP. LBs were stained with Erg6p-DsRed. Scale bar indicates 2 μm.

Figure 10. Mutations in the C-terminal extension do not affect the stability of Sna2p

GFP-Sna2p and GFP-Sna2p^{Y65/75A} were expressed in SCY62 strain. Protein biosynthesis was inhibited by the addition of cycloheximide and degradation rate of those proteins was assessed by immunoblotting at different time points : 0, 30, 60, 120 and 180 min (see materials and methods for details). Anti-Sna3p and anti-Cdc48p were used respectively as positive (Sna3p is targeted to the vacuolar interior and rapidly degraded) and negative (Cdc48p is a stable protein) controls.

Figure 11. A model for Sna2p trafficking and topology. Sna2p enters the secretory pathway at the level of the ER. Both YXXØ motifs are important for efficient Sna2p ER exit. If at least one of the motifs is mutated, Sna2p ER exit is decreased and the protein is redirected to nascent lipid bodies. At the level of the Golgi apparatus, both YXXØ motifs play a role in Sna2p targeting to the vacuole : Y₆₅XXØ mediates Sna2p targeting via the AP-1 pathway (through endosomes), while Y₇₅XXØ mediates targeting via the direct AP-3 pathway (bypassing endosomes). If at least one of the two motifs is mutated, Sna2p is redirected "by default" from the Golgi to the plasma membrane. The upper part of the figure shows a model of Sna2p topology in a phospholipid bilayer. Each residue is coloured according to its characteristics (neutral – nonpolar, neutral – polar, acidic, basic). Membrane domains were predicted using TMHMM software. As membrane proteins that reach lipid bodies must be monotopic, we depict Sna2p hypothetically embedded in only one leaflet of the phospholipid bilayer. Prolines and glycines might introduce kinks in the membrane domains that could favour this topology.

Figure 1

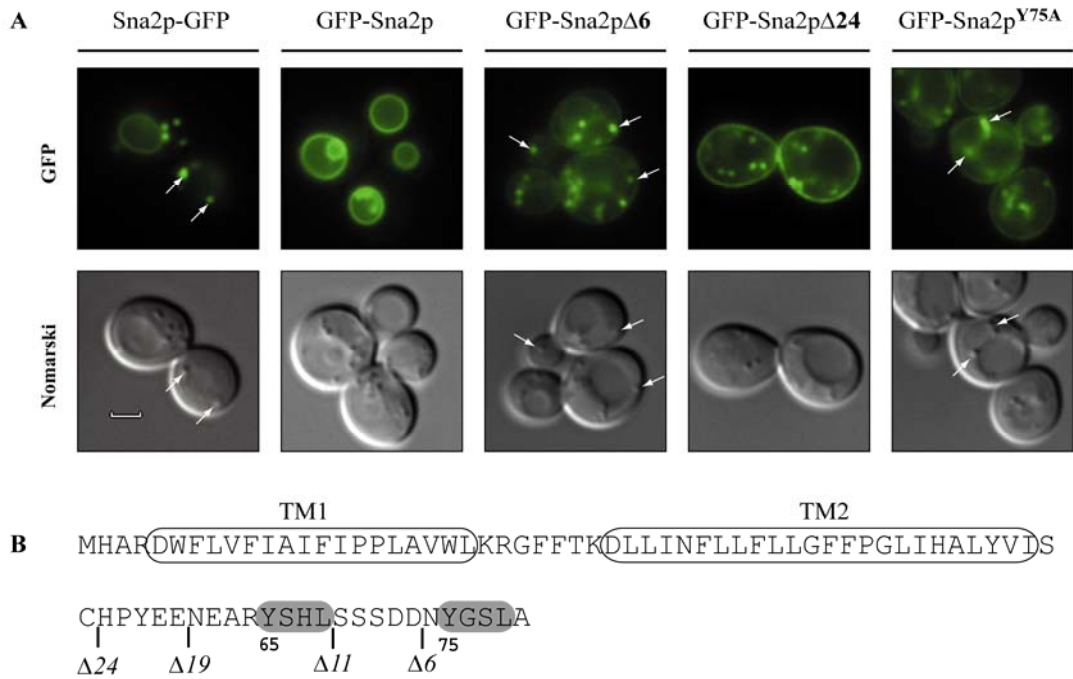
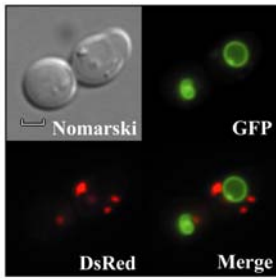


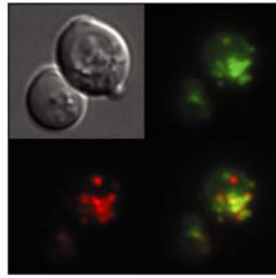
Figure 2

Non-fixed cells

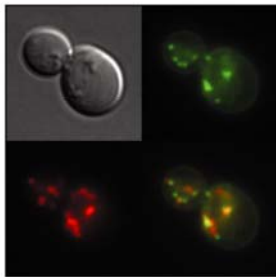
A. GFP-Sna2p



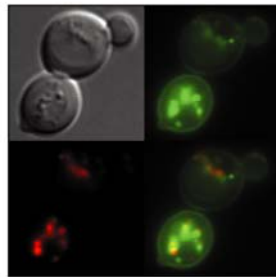
B. Sna2p-GFP



C. GFP-Sna2p Δ 6

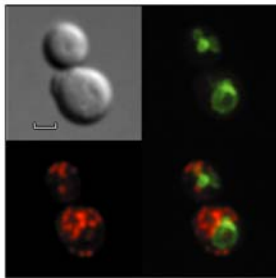


D. GFP-Sna2p^{Y75A}



Fixed cells (4% formaldehyde)

E. GFP-Sna2p



F. GFP-Sna2p Δ 6

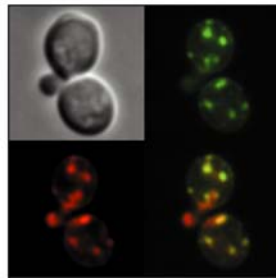


Figure 3

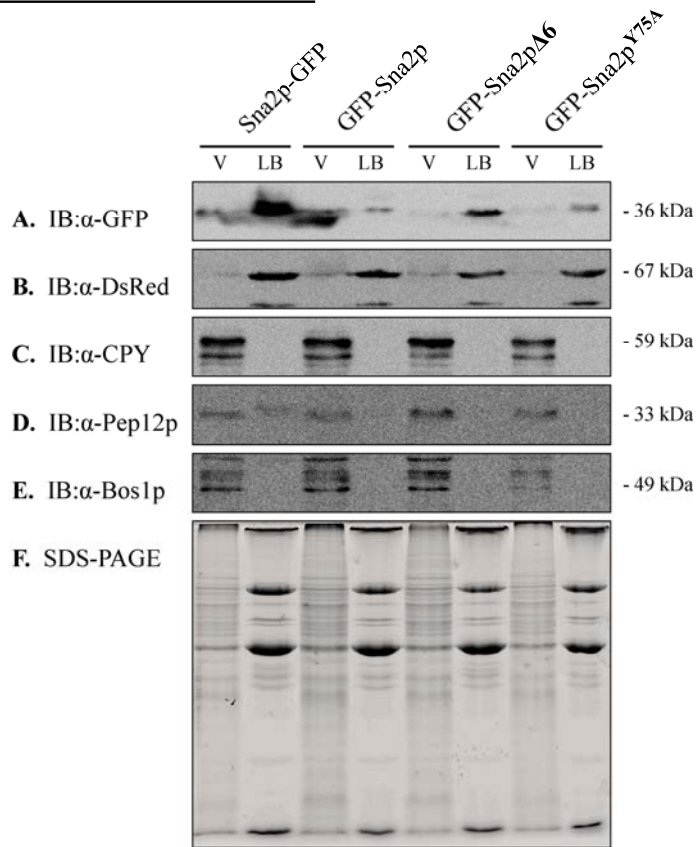


Figure 4

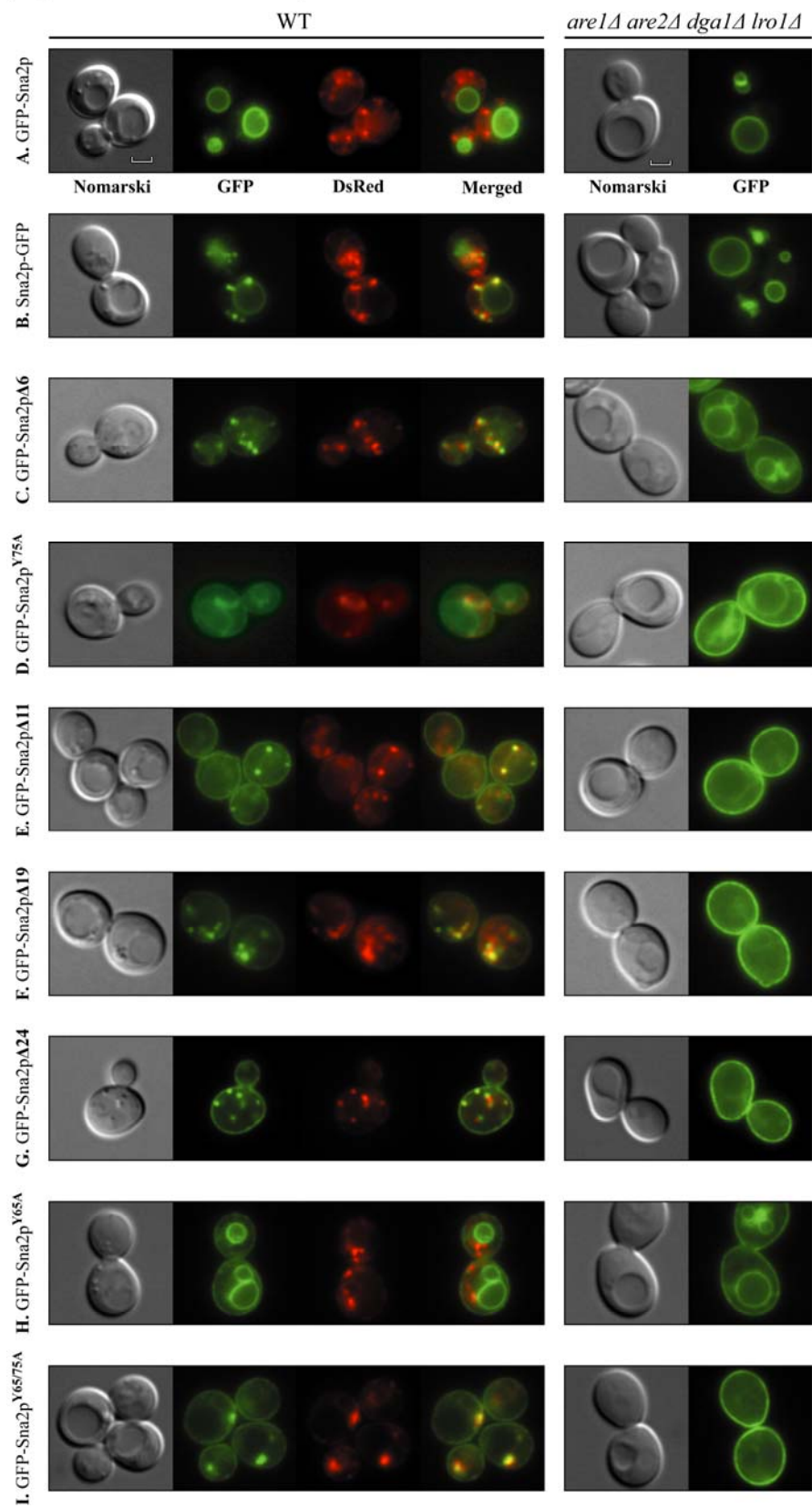


Figure 5

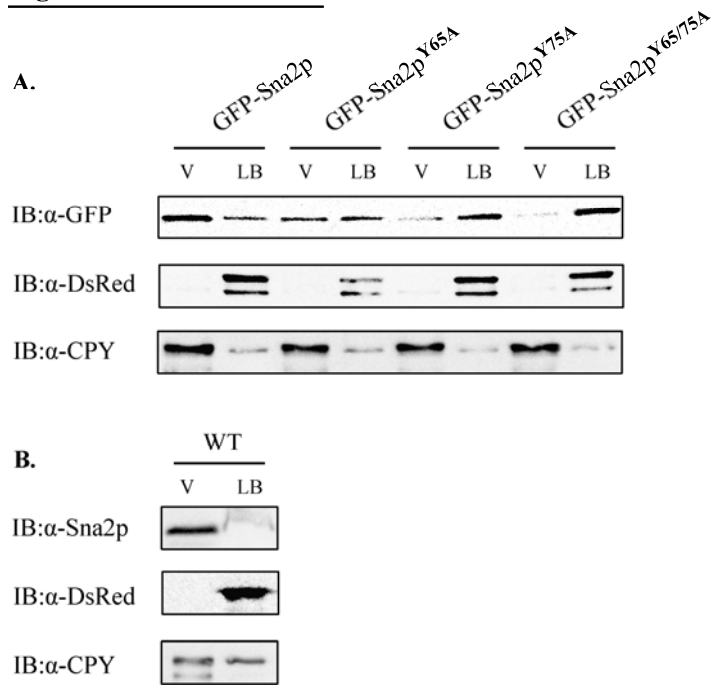


Figure 6

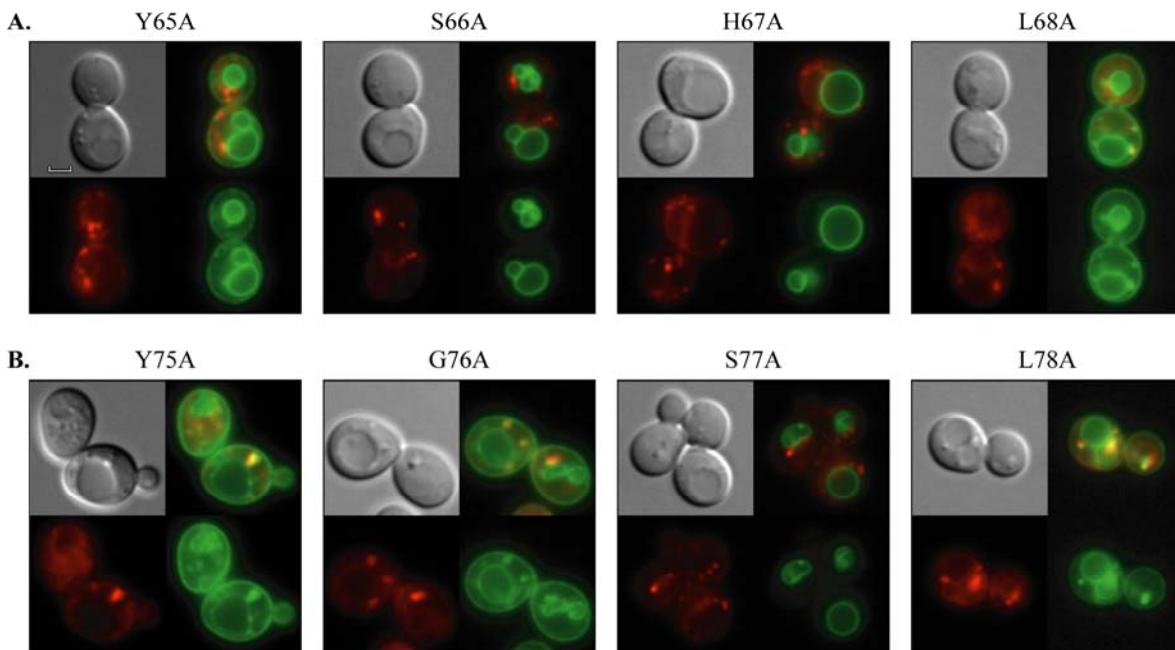


Figure 7

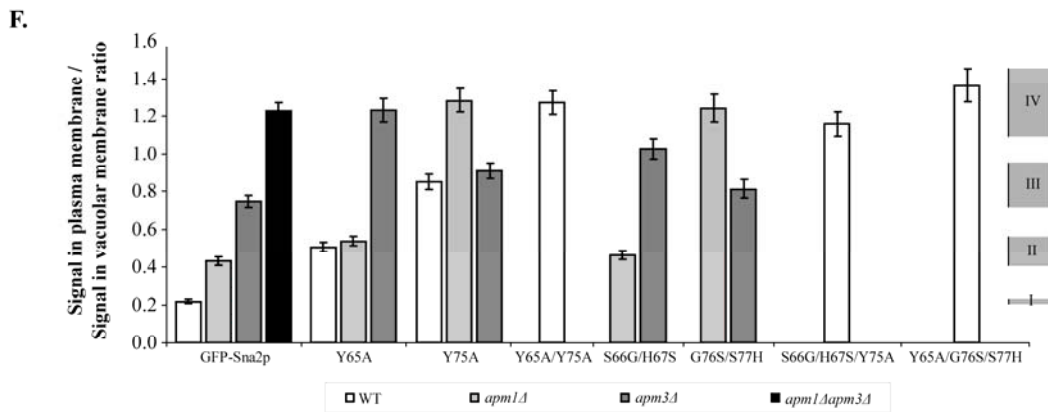
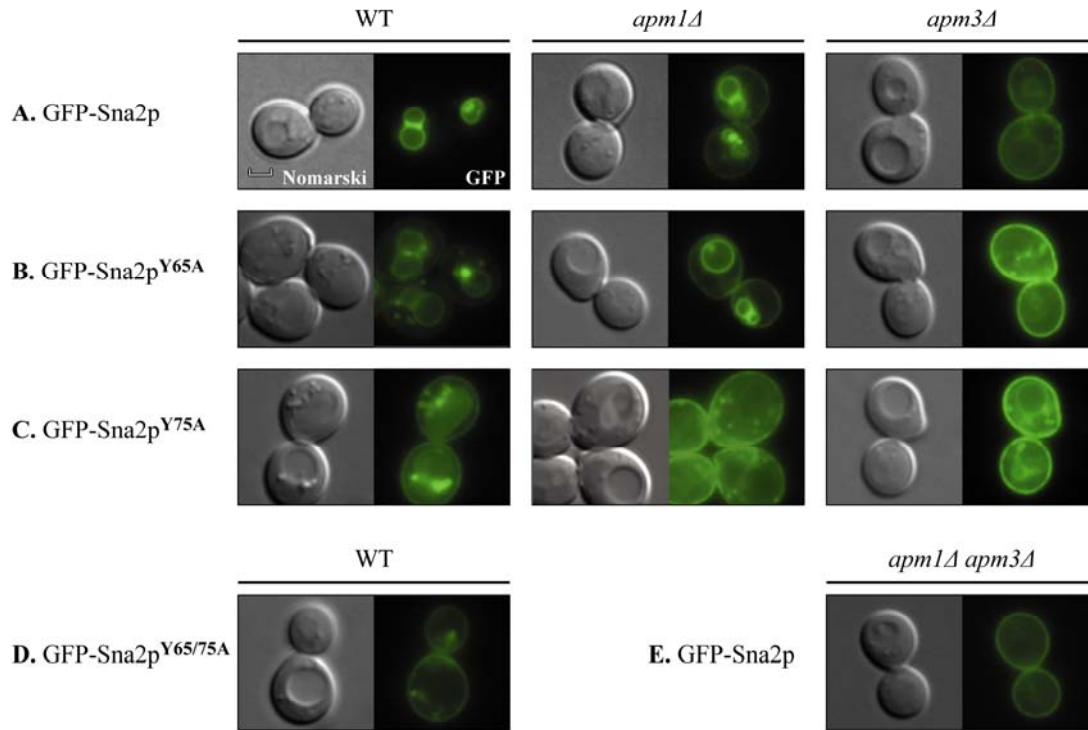


Figure 8

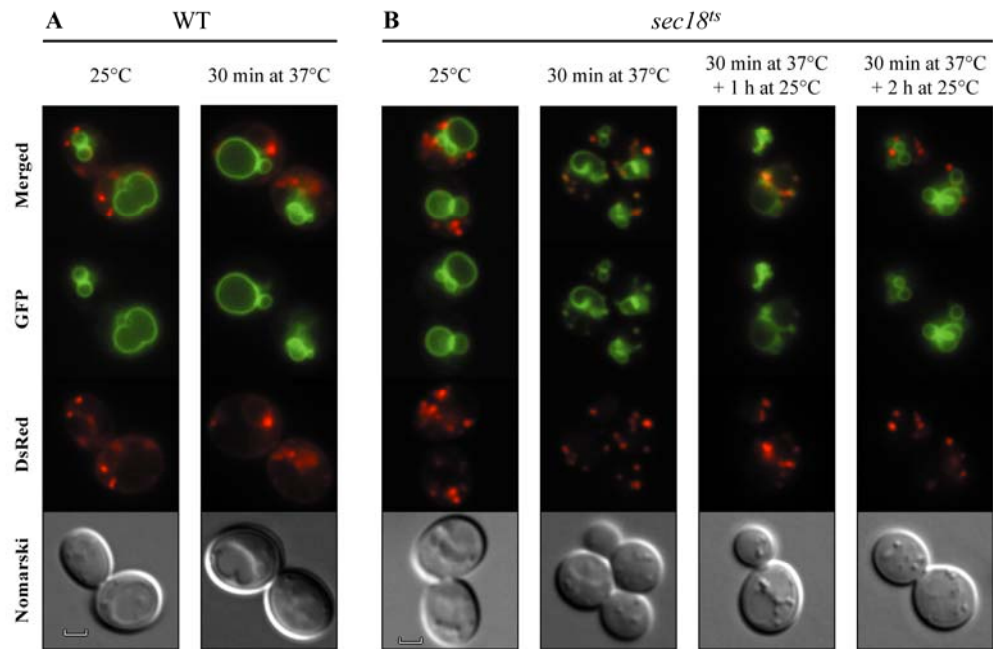


Figure 9

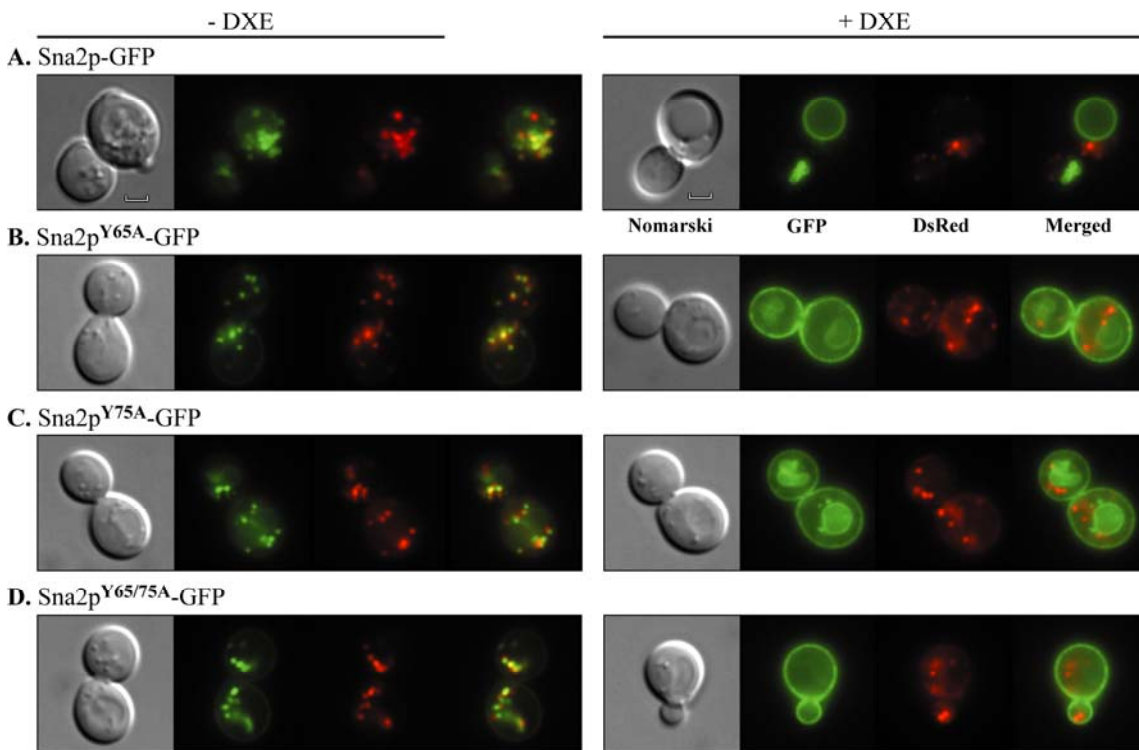


Figure 10

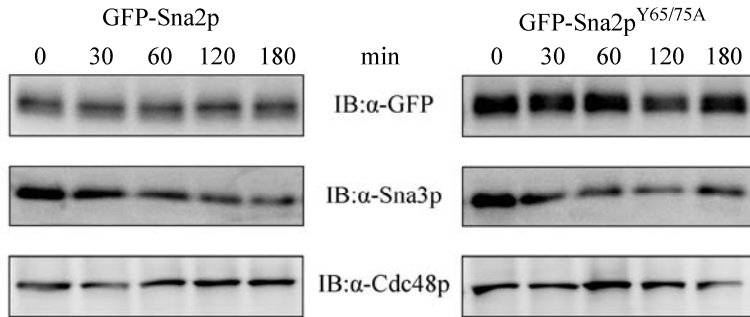


Figure 11

